Steel and Composite Structures, *Vol. 25, No. 3 (2017) 375-388*
DOI: https://doi.org/10.12989/scs.2017.25.3.375

Mechanical behavior of elliptical concrete-filled steel tubular stub columns under axial loading

Fa-xing Ding[1], Xing-zhi Ding[1], Xue-mei Liu[2], Hai-bo Wang[*1], Zhi-wu Yu[1,3] and Chang-jing Fang[1]

[1]*School of Civil Engineering, Central South University, Changsha, Hunan Province, 410075, P. R. China*
[2]*Schoo of Civil Engineering and Built Environment, Queensland University of Technology, Brisbane, QLD 4001, Australia*
[3]*National Engineering Laboratory for High Speed Railway Construction, Changsha 410075, China*

(*Received March 24, 2017, Revised July 20, 2017, Accepted August 08, 2017*)

Abstract. This paper presents a combined experimental, numerical, and analytical study on elliptical concrete-filled steel tubular (E-CFT) and rebar-stiffened elliptical concrete-filled steel tubular (RE-CFT) subjected to axial loading. ABAQUS was used to establish 3D finite element (FE) models for the composite columns and the FE results agreed well with the experimental results. It was found that the ultimate load-bearing capacity of RE-CFT stub columns was 20% higher than that of the E-CFT stub columns. Such improvement was attributed to the reinforcement effects from the internal rebar-stiffeners, which effectively enhanced the confinement effect on the core concrete, thereby significantly improved both the ultimate bearing capacity and the ductility of the E-CFT columns. Based on the results, equations were also established in this paper to predict the bearing capacities of E-CFT and RE-CFT stub columns under axial loading. The predicted results agreed well with both experimental and numerical results, and had much higher accuracy than other available methods.

Keywords: rebar-stiffened; elliptical concrete-filled steel tubular (E-CFT); finite element analysis (FEA); Ultimate bearing capacity

1. Introduction

Both circular and square concrete-filled steel tubular (CFT) columns are gaining increased applications in modern construction practices considering their higher stiffness, higher ultimate load-bearing capacity and ductility than conventional reinforced concrete columns. Elliptical concrete-filled steel tubular (E-CFT) columns are attracting more attentions in recent years for their attractive appearance and high flexibility in contrast to both square and rectangular CFT columns.

Elliptical profile sections are now available with outer dimensions ranging from 150×75 mm to 500×250 mm with thicknesses ranging from 4 mm to 16 mm and an aspect ratio at 2 according to EN10210 (2006a, b). Numerous experimental and numerical studies on the mechanical performance of E-CFT columns under the axial compressive loads are available from literatures. An experimental study on 21 normal E-CFT columns under uniform axial compression has been conducted by Yang *et al.* (2008) to study the effects of steel tube thickness, concrete strength and constraining factor on elastic stiffness, ductility, and ultimate strength. The results showed the axial compressive behavior of E-CFT columns was in between that of square or rectangle CFT columns and circular CFT columns. EC4 design code for square and rectangle CFT columns was proposed to be adopted for E-CFT columns by Yang *et al.* (2014), Jiang *et al.* (2013) (2013) reported a finite element analysis of the axial compressive behavior of concrete-filled steel tubular slender columns with elliptical section. Jamaluddin *et al.* (2013) presented an experimental study on E-CFT stub and slender columns. Various column lengths, sectional sizes and infill concrete strengths were used to quantify the influence of member geometry and constituent material properties on the structural behavior of E-CFT columns. New equations based on EC4 provisions for concrete filled hollow sections were proposed and used to predict the capacities of E-CFT columns. Zha *et al.* (2013) proposed a unified formula for the axial compressive strength of E-CFT columns according to finite element (FE) and theoretical analysis. Uenaka (2014) investigated the characteristics of CFEST stub columns under centric loading, and proposed a method to predict the axial loading capacity induced by confinement effects of the in-filled concrete. Dai *et al.* (2014) presented a non-linear finite element model and used it to predict the behavior of slender concrete filled steel tubular (CFST) columns with elliptical hollow sections subjected to axial compression. It was concluded that the design rules given in EC4 design code for circular and rectangular CFST columns may be adopted to calculate the axial buckling load of elliptical CFST columns. Qiu *et al.* (2017) conducted a numerical model simulating the behavior of elliptical concrete-filled columns under either concentric or eccentric compressive load, and an assessment is made of the reliability of the design proposals for concrete-filled elliptical hollow section columns. However, with the authors' best knowledge, there is no available

*Corresponding author, Ph.D.,
E-mail: haibarg@163.com

ISSN: 1229-9367 (Print), 1598-6233 (Online)

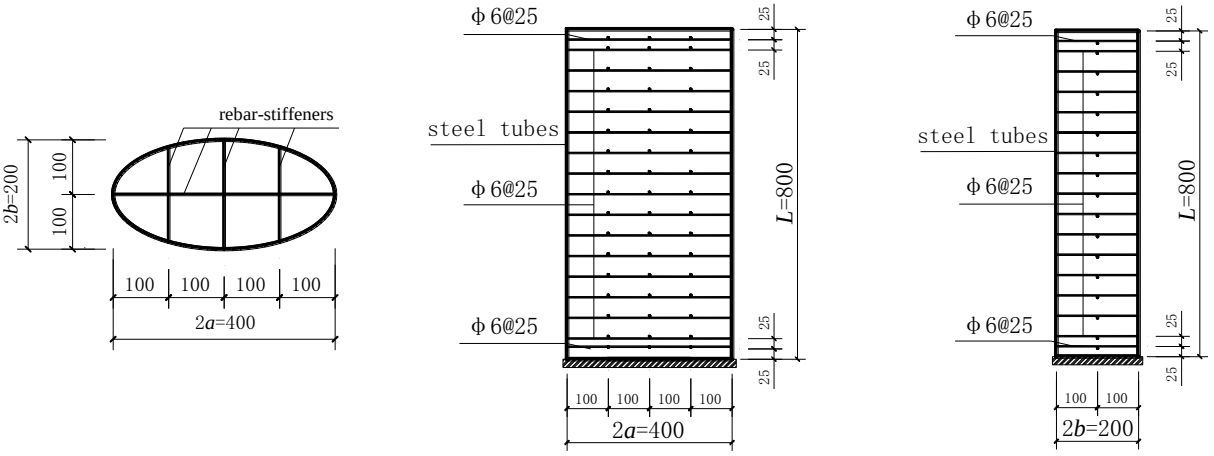

(a) Plan (b) Side view (c) Elevation

Fig. 1 Processing map of RE-CFT stub column

Table 1 Geometric properties and characteristics of CFT stub columns

Specimen number	$2a\times2b\times t$ /mm	L /mm	d /mm	f_{cu} /MPa	f_s /MPa	f_t /MPa	Steel ratio ρ	N_{u0} /kN	N_{u0} Increase percentage	DI
OVST1-A	408×191×3.78	800	—	35.5	311	—	0.057	3100	—	4.548
OVST1-B	409×190×3.70		—			—	0.056	2860	—	5.361
OVST2-A	404×195×5.81		—		321	—	0.087	3690	—	3.631
OVST2-B	407×196×5.84		—			—	0.087	3810	—	4.849
OVST3-A	406×189×3.71		—	54.4	311	—	0.057	3900	—	4.289
OVST3-B	405×194×3.77		—			—	0.057	3900	—	3.103
OVST4-A	405×195×5.80		—		321	—	0.086	4390	—	4.553
OVST4-B	402×198×5.89		—			—	0.087	4110	—	5.656
OVRST5-A	401×199×3.78		6	35.5	311	435	0.064	3720	24.8%	5.250
OVRST5-B	401×200×3.80						0.064	3610	21.1%	6.950
OVRST6-A	400×200×3.72			54.4			0.063	4550	21.3%	4.997
OVRST6-B	403×197×3.67						0.063	4500	20.0%	6.345

Note: N_{u0} is the ultimate bearing capacity from tested results; $\rho=A_s/A_{sc}$, A_s is area of steel tube and A_{sc} is the total area of cross-section.

formula in any Code of Practice to guide the calculation on the axial compressive strength of E-CFT columns.

Previous researches showed that the central concrete attained poor constraint from elliptical steel tube. In order to enhance the confinement effect on the core concrete and increase the bearing capacity and ductility of the square CFT stub columns, both experimental study and theoretical analysis were carried out in the reference (Xiamuxi *et al.* 2011, Park *et al.* 2013, Ding *et al.* 2014, Yang *et al.* 2014, Li *et al.* 2016, Su *et al.* 2016, Wang *et al.* 2017) by setting different constraint types inside the steel tube. One of those constraints, the rebar-stiffener, could be applied to E-CFT stub columns.

To date, researches have been focused on rebar-stiffener CFT stub columns in rectangle, square, and round-ended shapes. Very limited studies can be found on rebar-stiffened elliptical CFT (RE-CFT) stub columns.

Therefore, this paper aims to study the elliptical CFT stub columns and propose an approach to estimate the ultimate bearing capacity of the E-CFT and RE-CFT stub columns. More specifically the following objectives were included in this study. (1) To experimentally study the behavior of both E-CFT and RE-CFT stub columns under axial loading; (2) To numerically evaluate the behavior of both E-CFT and RE-CFT stub columns under axial loadings through 3D finite element analysis (FEA) using ABAQUS software; (3) To investigate the effect of rebar-stiffeners on the mechanical performance of stub columns; (4) To establish a simplified and accurate approach to estimate the ultimate bearing capacity of both E-CFT and RE-CFT stub columns.

Table 2 Mix design of concrete

Concrete strength level (MPa)	Cement (kg/m^3)	Sand (kg/m^3)	Water (kg/m^3)	Gravel (kg/m^3)
C30	429	536	185	1250
C50	478	610	172	1186

Table 3 Mechanical properties of steel

Thickness/Diameter	Yield strength f_y/MPa	Ultimate strength f_u/MPa	Elastic modulus E_s/MPa	Poisson's ratio v_s
4 mm	311	460	207000	0.293
6 mm	321	480	209000	0.286
φ6	435	615	210000	0.294

2. Experimental investigation

2.1. General

Total 12 specimens were designed and tested in this study, including 8 E-CFT and 4 RE-CFT stub columns to study the influence of different parameters including rebar stiffener, concrete strength, and steel ratio on the mechanical performances of E-CFT and RE-CFT stub columns. The cross section and section profiles of stub columns are shown in Fig. 1. The geometric properties and the mechanical characteristics of all columns are presented in Table 1. The nominal dimension of each specimen is 400 (2a) mm ×200 (2b) mm × 4(6) (t) mm × 800 (L) mm. In Table 1, 2a is the major outside width of elliptical section, 2b is the minor outside width of elliptical section, t is the wall thickness of the steel tube, L is the height of the specimen, d is the diameter of rebar-stiffeners, f_{cu} is cube concrete strength of concrete, f_s is yield strength of steel, f_t is yield strength of rebar-stiffeners, ρ is steel ratio of specimen and $N_{u,0}$ is axial ultimate bearing capacity of specimen.

Red paint was sprayed on the external surface of the steel tubes and grids of 50×50 mm were drawn on the painted surface for better observation of deformation and local failure of the columns before preparing the columns. The elliptical steel tube was firstly welded together with the cover plate. Then the concrete was poured into the tubes from the top of the specimens and carefully vibrated to compact the concrete. After that, the top surface of concrete was smoothened and leveled at the same level with the steel tube. Meanwhile, standard concrete cubes at 150×150×150 mm were also prepared for material testing and cured in the same condition as the concrete used in the E-CFT and RE-CFT stub columns. After cured for one month, the concrete surfaces of the columns were polished with grinder, and then steel cover plates were bonded at the top end of the columns by applying a layer of epoxy resin binder to ensure that the steel tube and core concrete shared loads from the initial loading stage.

2.2 Material properties

Commercial pump concretes of grade C30 and C50 were used for E-CFT and RE-CFT columns and the mix ratios are summarized in Table 2. Concrete cubes were tested according to GB/T50081-2016 and the obtained cubic strength f_{cu} was 35.5, and 54.4 MPa, respectively.

The elliptical steel tubes were molded by bending Q235 steel plates into half-oval and then welding the two half-sections. Rebar-stiffeners were also welded with the steel tubes. The ordinary hot-rolling steel is adopted, and it is bent and formed on the bending press. Butt welds were designed according to GB/50017-2014, and heat-treatment had been carried out, so residual stresses should not be included. The properties of the weld could be the same as the parent material in the numerical analysis. Standard coupon specimens, 4 mm-thick and 6 mm-thick steel plates and φ6 steel bars were prepared. Tensile tests were carried out according to GB/T228-2010. The obtained material properties of the steel plates and bars are presented in Table 3.

2.3 Experimental setup and instrumentation

Compressive test on E-CFT and RE-CFT stub columns were conducted using a 500-ton triaxial stress testing machine in the Civil Engineering Safety Science Laboratory of Central South University. To accurately measure the deformation, four strain rosettes (A# to D#) were installed at the mid-height of the steel surface and two LVDTs were installed at the same height of two opposite side surfaces along short axis, as shown in Fig. 2(a). Load-strain curves were acquired by a DH3818 static strain measurement system and load-deformation curves were acquired from electronic transducers and RX-24A data acquisition system.

Fig. 2(b) shows the actual experimental setup. Before testing, specimens were centered and pre-loaded to ensure the evenness of the loading surface. Then the compressive load was applied from the top of the specimen using multi-step loading mode. The load was increased at a step of 1/10 of the ultimate capacity in the elastic stage and at the step of 1/20 of the ultimate capacity in the elastic-plastic stage.

Each loading step took 5-7 min and testing data were collected in each step. Before the ultimate capacity was approached, specimens were loaded slowly and continuously until final failure. Each specimen took about 3 hours for testing.

3. Experimental results and discussions

3.1 Load-deformation responses and failure modes

For E-CFT stub columns, in the early period of loading, the specimens were in elastic stage, indicated by the linear load-displacement curves and inconspicuous change of steel surface. When the applied load reached 60~70 percent of the ultimate load, the specimens began to be in the elastic-plastic stage, indicated by the decrement of the stiffness with the load-displacement curves decreasing gradually and the local buckling of the steel tube appeared. When the ultimate load was approached, with the concrete damaged, the load-deformation curves declined quickly and the steel tubes yielded at the middle of the specimens. The test was then stopped due to the large transformation of specimens.

For RE-CFT stub columns, the experimental performance was similar to those E-CFT columns before reaching the ultimate load. With continued loading, some rebar-stiffeners were broken with noises. The descent rate of RE-CFT bearing capacities was significantly slowed down and the ductility observably increased compared with those of E-CFT stub columns.

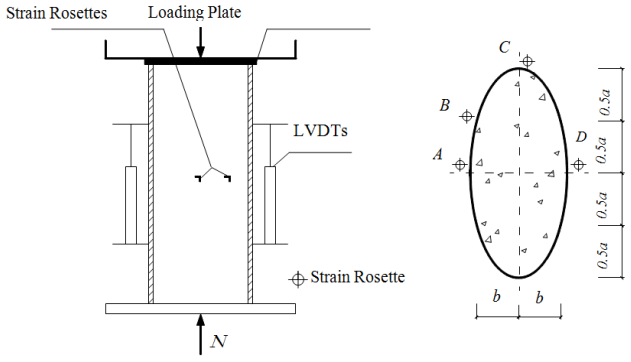

(a) Experimental instrumentation

(b) Test specimen

Fig. 2 Test specimen and instrumentation

Fig.3 shows the failure mode of the typical tested specimens and the inner concretes. It indicated that the RE-CFT steel tubes yielded at the middle of the specimens while the E-CFT tubes yielded at the top. The ultimate bearing capacities of all specimens are summarized in table 1 and the load-deformation curves of all specimens are shown in Fig. 4.

(a) RE-CFT stub column

(b) E-CFT stub column

(c) Core concrete of E-CFT stub column

Fig. 3 Typical failures of specimens

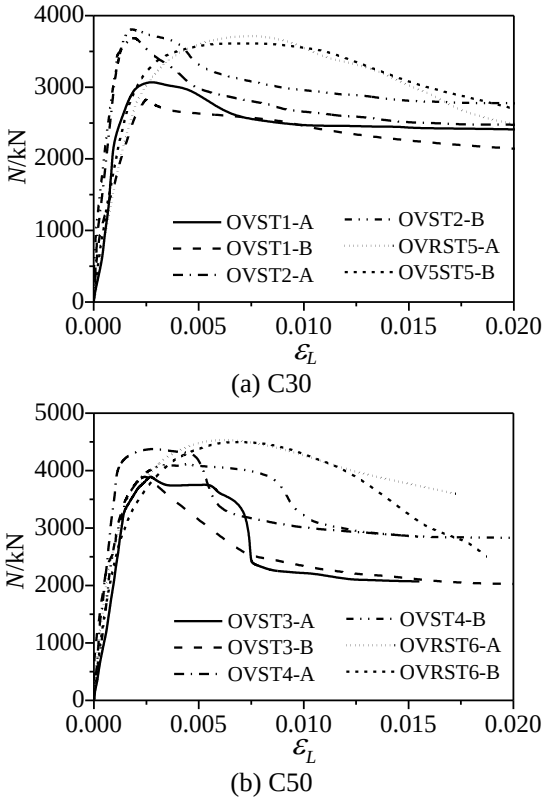

(a) C30

(b) C50

Fig. 4 Load (N) versus strains (ε_L) curve of all specimens

3.2 Load bearing capacity

Fig. 5 compares the different ultimate bearing capacities of all specimens. In comparison to the specimens OVST1 (t=4 mm, f_{cu}=35.5 MPa), the ultimate bearing capacity of specimens OVST2 (t=6 mm, f_{cu}=35.5 MPa) was increased by 19.0% - 33.2%, with a 55.4% increase of steel ratio. While in comparison to the specimens OVST3, the ultimate bearing capacity of specimens OVST4 was only increased by 5.4% - 12.6%, with the 55.4% increase of steel ratio. It indicated that an increase of steel ratio can yield an improvement of the ultimate bearing capacity of the E-CFT columns; yet, the increase amplitude tended to decrease with the increased concrete compressive strength.

In comparison to the specimens OVST1 (t=4 mm, f_{cu}=35.5 MPa), the ultimate bearing capacity of specimens OVST3 (t=4 mm, f_{cu}=54.4 MPa) was increased by 25.8% - 36.4%, with a 53.2% increase of concrete strength. While in comparison to the specimens OVST2 (t=6 mm, f_{cu}=35.5 MPa), the ultimate bearing capacity of specimens OVST4 (t=6 mm, f_{cu}=54.4 MPa) was only increased by 7.9% - 19.0%, with a 53.2% increase of concrete strength. It indicated that an increase of concrete strength can yield an improvement of the ultimate bearing capacity of the E-CFT columns; yet, the increase amplitude tended to decrease with the increased steel ratio.

In comparison to specimens OVST1 (t=4 mm, f_{cu}=35.5 MPa), the ultimate bearing capacity of specimens OVRST5 (t=4 mm, f_{cu}=35.5 MPa, d=6 mm) was increased by 21.1% - 24.8%, with a 0.82% increase of rebar-stiffeners ratio. While in comparison to specimens OVST3 (t=4 mm, f_{cu}=54.4 MPa), the ultimate bearing capacity of specimens OVRST5 (t=4 mm, f_{cu}=54.4 MPa, d=6 mm) was increased by 20.0% - 21.3%, with a 0.82% increase of rebar-stiffeners ratio. It indicated that an increase of rebar-stiffeners ratio can also yield an improvement of the ultimate bearing capacity of stub columns and the increase amplitude was not significantly influenced by the concrete strength.

The average ratio of the ultimate bearing capacities of specimens OVRST5 (ρ=0.087, f_{cu}=35.5 MPa) to those of OVST2 (ρ=0.064, f_{cu}=35.5 MPa) was 0.998, while the average ratio of specimens OVRST6 (ρ=0.064, f_{cu}=54.4 MPa) to OVST3 (ρ=0.087, f_{cu}=54.4 MPa) was 1.065. It indicated that the ultimate bearing capacities of RE-CFT stub columns were very similar to those of E-CFT stub columns with higher steel ratios.

3.3 Ductility

To investigate ductility property of E-CFT and RE-CFT stub columns, a ductility index (DI), which has been used in the previous study on the inner constrained square CFT (Ding *et al.* 2014), is adopted. The corresponding ductility index is defined as follows:

$$DI = \frac{\varepsilon_{0.85}}{\varepsilon_y} \tag{1}$$

where $\varepsilon_{0.85}$ is the axial strain when the load falls to 85% of the ultimate load; ε_y is equal to $\varepsilon_{0.75}/0.75$, and $\varepsilon_{0.75}$ is the axial strain when the load attains 75% of the ultimate load in the pre-peak stage.

The ductility index obtained from Eq. (1) for all specimens is listed in Table 1 and the comparison between each other is shown in Fig. 6. In this figure, the influence of rebar-stiffeners on DI is identified. The RE-CFT specimens generally showed improved ductility in comparison to E-CFT ones, with average DI values of 4.955 and 4.420 for specimens OVST1 and OVST2 respectively, and with average DI values of 6.100 and 5.671 for specimens OVRST5 and OVRST6 respectively. Such results suggest that the ductility of specimens decreases with the increase of concrete strength. More importantly, it was found that the inner rebar-stiffeners were efficient to increase the ductile performance for elliptical concrete-filled steel tubes.

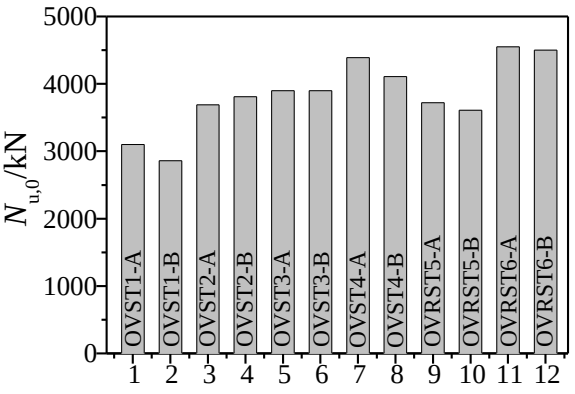

Fig. 5 Comparison of ultimate bearing capacity for all specimens

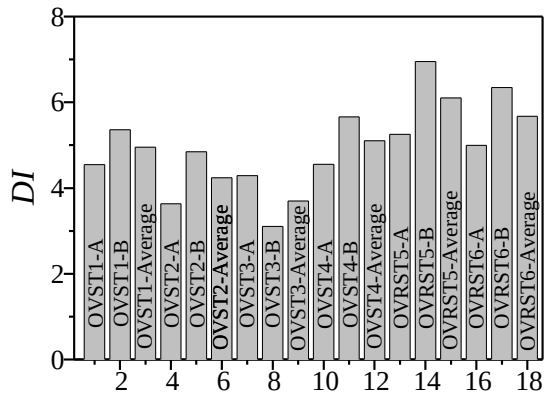

Fig. 6 Comparison of ductility index DI for all specimens

4. Finite element (FE) modeling

4.1 FE models

FE models were established using ABAQUS program (Hibbitt *et al*. 2014). In these models, three-dimensional 8-node reduced integral format solid elements (C3D8R) were used for the core concrete and the rigid loading plate, and 4-node reduced integral format shell elements (S4R) were adopted for the elliptical steel tube to ensure the computation accuracy according to Ding *et al.* (2014). Moreover, 2-node linear 3-D truss elements were used for internal rebar-stiffeners. Mesh was divided by a structural grid dividing technology. And mesh convergence studies were first performed to ensure FEA could provide accurate results. The established FE model was shown in Fig. 7.

The concrete constitutive relationship and the value of corresponding parameters were suggested by Ding *et al.* (2011a)

$$y=\begin{cases}\dfrac{kx+(m-1)x^2}{1+(k-2)x+mx^2} & x\le 1\\ \dfrac{x}{\alpha_1(x-1)^2+x} & x>1\end{cases} \tag{2}$$

where, $y=\sigma/f_c$, $x=\varepsilon/\varepsilon_c$; σ is the axial stress of core concrete with unit MPa; f_c is the uniaxial compressive strength of concrete, $f_c=0.4f_{cu}^{7/6}$; ε is the axial strain of core concrete; ε_c is the strain corresponding with the peak compressive stress of concrete, $\varepsilon_c = 383\, f_{cu}^{7/18}\times 10^{-6}$; k and m are adopted for the ascending branch, $k=9.1\, f_{cu}^{-4/9}$, $m = 1.6(A_1 - 1)^2$; parameter α_1 adopted for the descending branch can be taken as 0.15.

A small amount of stress-strain data was taken while the strain is smaller. It has little influence on the calculation results at elastic stage, but it is easy to calculate and converge.

An elastic-plastic model was used to describe the constitutive behavior of steel. The expression for the stress-strain relationship of steel and rebar is as below (Ding *et al.* 2011a)

$$\sigma_i=\begin{cases}E_s\varepsilon_i & \varepsilon_i\le\varepsilon_y\\ f_s & \varepsilon_y<\varepsilon_i\le\varepsilon_{st}\\ f_s+\zeta E_S(\varepsilon_i-\varepsilon_{st}) & \varepsilon_{st}<\varepsilon_i\le\varepsilon_u\\ f_u & \varepsilon_i>\varepsilon_u\end{cases} \tag{3}$$

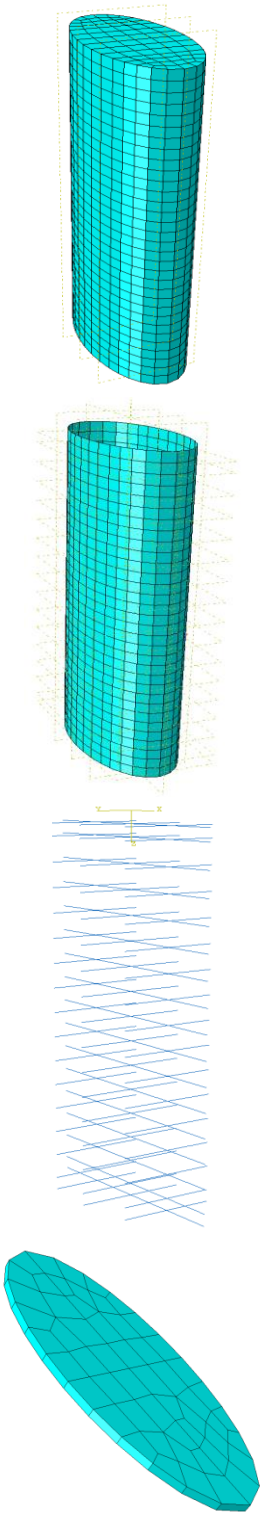

Fig. 7 Mesh refinement for FE models

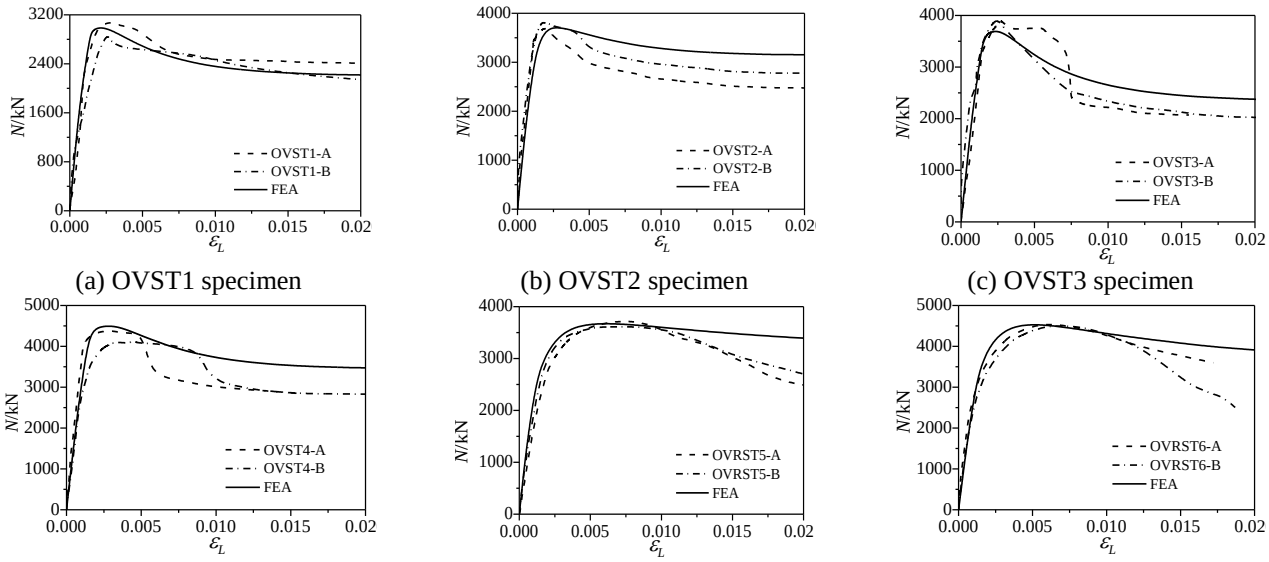

(a) OVST1 specimen (b) OVST2 specimen (c) OVST3 specimen

(d) OVST4 specimen (e) OVRST5 specimen (f) OVRST6 specimen

Fig.8 Comparison between calculated and tested curves on stub columns under axial compression

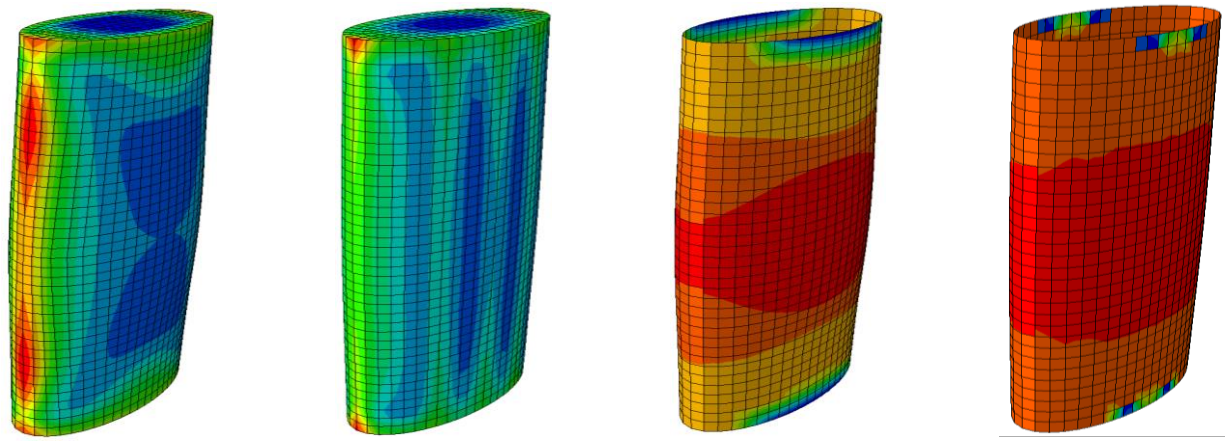

(a)E-CFT concrete (b)RE-CFT concrete (c) E-CFT steel tube (d) RE-CFT steel tube

Fig. 9 Failure mode of FEA model

where, σ_i is the equivalent stress of steel; f_s is the yield strength of steel; f_u is the ultimate strength of steel, $f_u = 1.5f_s$; E_s is the elastic modular of steel, $E_s = 2.06\times10^5$ MPa; ε_i is the equivalent strain of steel; ε_y is the yield strain of steel; ε_{st} is the hardening strain of steel, $\varepsilon_{st}=12\varepsilon_y$; ε_u is the ultimate strain of steel, $\varepsilon_u=120\varepsilon_y$; $\zeta=1/216$.

A pure master-slave surface contact was adopted for the constraint between steel tube (master surface) and concrete (slave surface) with finite slip formula. The interaction of the normal direction of the two surfaces was hard contact. The tangent contact was simulated by the Coulomb friction model, where the coefficient of friction used for E-CFT and RE-CFT stub columns under axial compression was 0.5 according to Dai *et al.* (2010), since they found that the coefficient of friction varying from 0.1 to 0.5 made little difference to the contact behavior. Core concrete and loading plate were tied together, and steel tube was constrained with loading plate by shell-to-solid coupling. For RE-CFT stub columns, steel tube was tie together with rebar stiffeners, which was embedded in core concrete. To model the decrease of load-bearing capacity of specimens, load was applied through increments of displacement.

4.2 Results and discussions

The ultimate bearing capacity of 12 specimens in this paper and the comparison between experiment and modeling results of 32 E-CFT stub columns sourced from literatures (only specimens with a/b=2) analyzed by ABAQUS are presented in Tables 5 and 7, where, $N_{u,0}$ is ultimate load-bearing capacity of CFET stub columns from tested results; $N_{u,1}$ is ultimate load-bearing capacity of CFET stub columns from FE results; $N_{u,2}$ is ultimate load-

bearing capacity of CFET stub columns from Eq. (13). The average value and the dispersion coefficient of $N_{u,0}/N_{u,1}$ of E-CFT columns (40 totals) are 1.006 and 0.056 respectively, and those of RE-CFT are 1.011 and 0.024 respectively, as shown in Tables 5 and 7. The comparison demonstrates that the numerical results are in good agreement with experimental results

Fig. 8 shows the comparison of load-axial strain curves of E-CFT and RE-CFT stub columns between FE modeling and experimental results. As seen in Fig. 8, good agreement between experimental and FE modeling results was found in the elastic stage. In the elastic-plastic stage and failure stage, strain values became large and increased very fast, which may contribute to the differences between the modeling and experimental curves. Fig. 9 shows the failure modes of both steel tube and the core concrete by FEA, which indicates that the axial compression behavior of RE-CFT columns is more balanced than that of E-CFT columns.

4.3 Confinement effect of rebar stiffeners

In order to study the influence of rebar stiffeners on the mechanical performance of E-CFT stub columns, the load-strain curves (N-ε_L) of both OVST1-A and OVRST5-A columns, and also the respective core concrete and steel tube, obtained by the numerical method were compared in Fig. 10. The results showed that the ductility of OVRST5-A specimen was significantly improved compared with specimen OVST1-A, with a 20% increase of ultimate bearing capacity. Load borne by steel tube of specimen OVRST5 is similar with the one of OVST1, while the load borne by the core concrete is much strengthened with the rebar stiffeners. It can be derived that the rebar stiffeners enhanced the concrete lateral restraint effects and largely increased the compression bearing capacity of the core concrete. Therefore, the ultimate bearing capacity and ductility of the stub columns were increased significantly. In sum, the mechanical performance of the RE-CFT stub columns was greatly improved compared with that of the E-CFT stub columns.

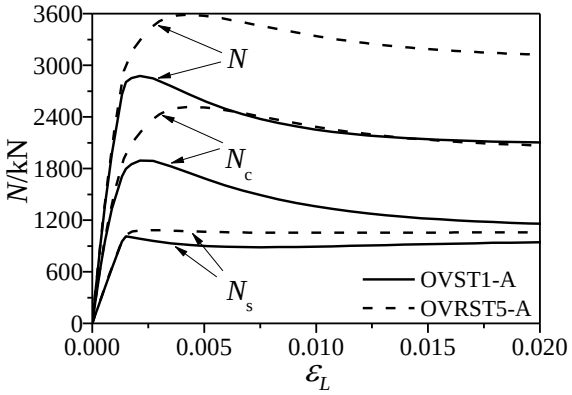

Fig. 10 Comparisons of Load (N) versus strains (ε_L) curve under axial loading

Fig. 11 shows the axial stress-strain curves ($\sigma_{\theta,s}$ - ε_L) and transverse stress-strain curves ($\sigma_{L,s}$ - ε_L) of the steel and the axial stress-strain curves ($\sigma_{L,c}$ - ε_L) of the concrete at the point A, B and C (Fig. 2) of the mid-section for OVST1-A and OVRST5-A, respectively. For E-CFT stub columns, the sequence of intersection between axial stress and transverse stress is point C, point B and point A. And the concrete axial stress at point C is larger than that at point A. The result indicates that the highest confinement effect was provided at the end of the principle axis (point C) and the least confinement effect was provided at the end of the minor axis (point A). For RE-CFT stub columns, the decrease rate of axial stress and the increase rate of hoop stress of steel tube at point A and B are weakened fast, yet which at the point C is almost constant after yielding, compared with E-CFT stub columns. It shows that the confinement effect of elliptical steel tube on core concrete is strengthened by rebar stiffeners, and at the end of minor axis, such strengthening effect is most significant. Therefore, rebar stiffeners covered the shortage of the confinement effect of steel tube on the core concrete along the minor axis.

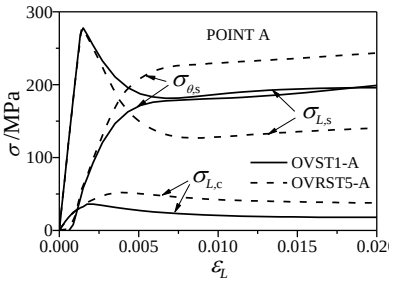

(a) Point A on elliptical steel tubes

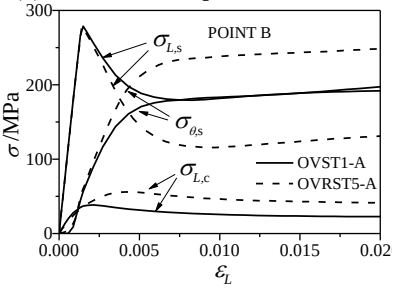

(b) Point B on elliptical steel tubes

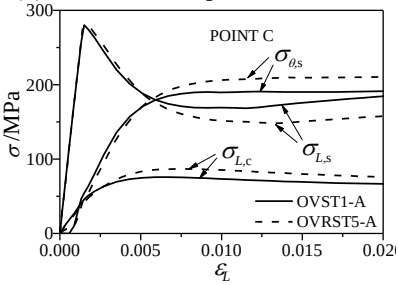

(c) Point C on elliptical steel tubes

Fig.11 Comparisons of steel longitudinal stress, steel hoop stress and concrete longitudinal stress versus strain (ε) curve between E-CFT and RE-CFT stub columns

5. Formula establishment for bearing capacity

5.1 Model simplification

A range of parameters such as concrete strength, steel ratio, steel yield strength, rebar stiffeners ratio, and rebar yield strength and their influences on the mechanical performance of E-CFT and RE-CFT columns were further investigated using FE modeling. These parameters commonly used in engineering practice include three steel strengths (235 MPa, 345 MPa and 420 MPa), three concrete strengths (40 MPa, 60 MPa and 80 MPa), three steel ratios (0.02, 0.05 and 0.08), and three rebar stiffeners ratios (0.005, 0.01, 0.015). 18 of E-CFT and 54 of RE-CFT FE models were thoroughly investigated. The dimensions of all specimens are as follows: column length L = 2400 mm, major outside dimension of elliptical section $2a$ = 1200 mm, minor outside dimension of elliptical section $2b$ = 600 mm. When the specimen reached their ultimate strength, axial stresses at the three point of the steel tube (A, B and C) were obtained and the relationship between axial stress-yield strength ratio and the specimens' ultimate strength (f_{sc} = N_u/A_{sc}, A_{sc} = A_c+A_s is total area of cross-section) are shown in Figs. 12 and 13.

It can be identified from Fig. 12 that when E-CFT stub columns reach their ultimate strength, the average value of the ratio of the steel tube's axial compressive stress to yield stress is

$$\sigma_{L,s} = 0.86 f_s \tag{4}$$

Based on Von Mises yield criterion, the tensile transverse stress ($\sigma_{\theta,s}$) of the steel tube can be obtained as

$$\sigma_{\theta,s} = 0.24 f_s \tag{5}$$

For RE-CFT stub columns, as shown in Fig. 13, the average values of the ratio of the steel tube's axial compressive stress ($\sigma_{L,s}$) under different rebar-stiffeners ratio and the tensile transverse stress ($\sigma_{\theta,s}$) to yield stress are listed in Table 4. In Table 4, ρ_v is rebar stiffeners ratios of column.

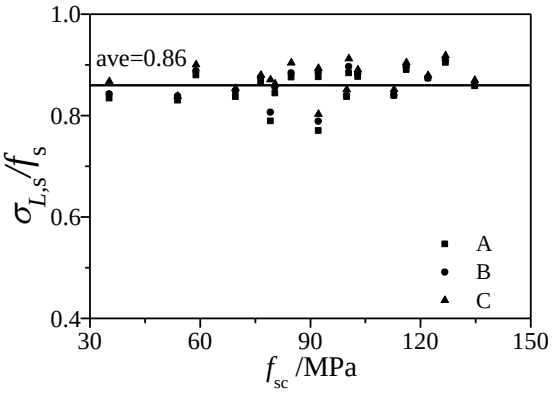

Fig. 12 Relationship between the ratio of various stresses versus the yield stress and the ultimate bearing strength for E-CFT stub columns

Table 4 Relationship between various stresses and yield stress for RE-CFT stub columns

ρ_v/ρ	$\sigma_{L,s}/f_s$	$\sigma_{\theta,s}/f_s$	k'
0	0.86	0.24	1.10
0.05	0.67	0.48	1.21
0.10	0.76	0.37	1.19
0.15	0.81	0.31	1.16

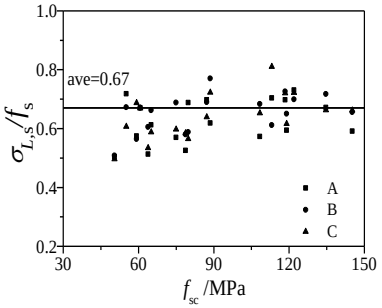

(a) ρ_v/ρ =0.05

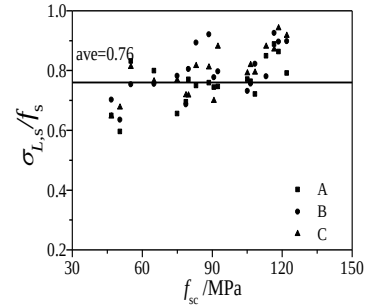

(b) ρ_v/ρ=0.10

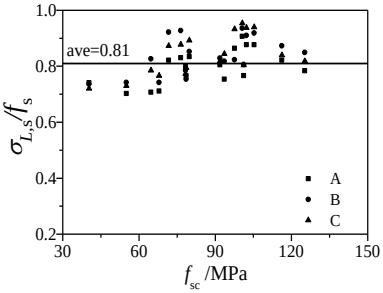

(c) ρ_v/ρ=0.15

Fig.13 Relationship between the ratio of various stresses versus the yield stress and the ultimate bearing strength for RE-CFT stub columns

The results of FE nonlinear numerical analysis indicate that the confinement effect on the core concrete obtained from elliptical steel tube was almost along the principle axis for E-CFT stub columns, and it was improved by rebar stiffeners along the minor axis for RE-CFT stub columns.

The stress contour at the ultimate state for core concrete was extracted from the FE modeling and was shown in Fig. 14. According to the stress contour at the ultimate stage shown in Fig. 14, the stress distribution of core concrete of E-CFT and RE-CFT columns is simplified in Fig. 15.

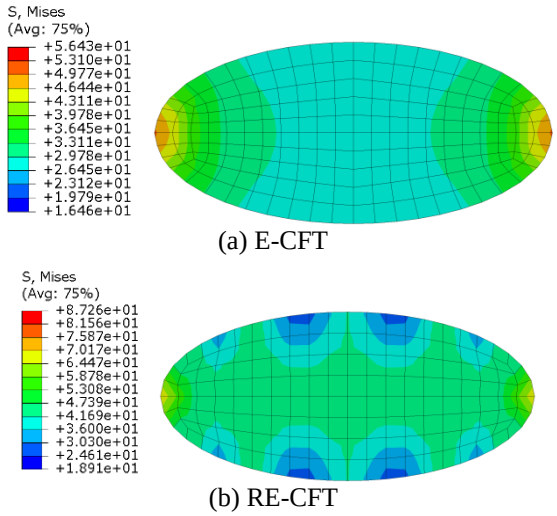

Fig. 14 Stress contours at mid-section for E-CFT and RE-CFT stub columns

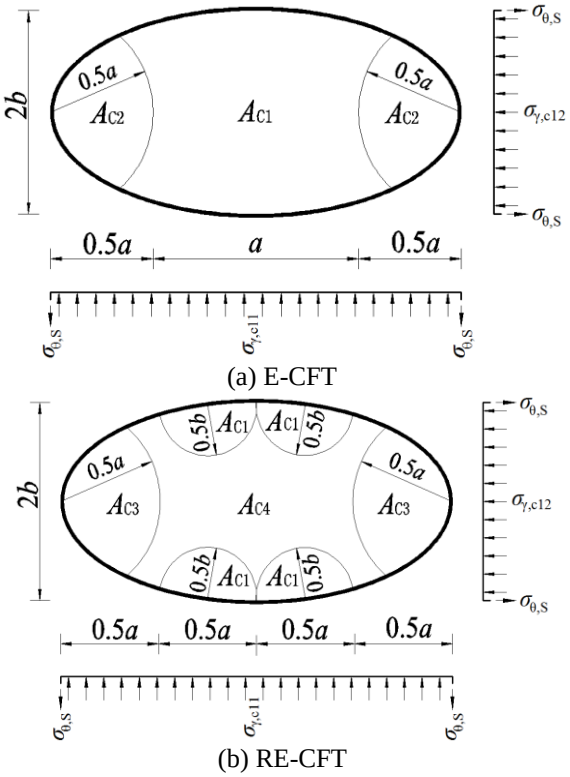

Fig. 15 Simplified stress distribution at mid-section for E-CFT stub column

In Fig. 15 (a), A_{c1} is the unconstrained concrete area, and A_{c2} is the area constrained by elliptical steel tube. In Fig. 15(b), A_{c1} is also the unconstrained concrete area, A_{c3} is the area constrained by both elliptical steel tube and rebar stiffeners, and A_{c4} is the area constrained by rebar-stiffeners only. In this way, the following relationship for E-CFT stub columns can be obtained:

$$\begin{cases} A_{c1} = 0.67A_c \\ A_{c2} = 0.33A_c \end{cases} \tag{6a}$$

For RE-CFT stub columns, the relationship is

$$\begin{cases} A_{c1} + A_{c3} + A_{c4} = A_c \\ A_{c3} = 0.33A_c \\ A_{c4} = 0.40A_c \\ A_{c3} + A_{c4} = A_{cor} \end{cases} \tag{6b}$$

where A_c is the core concrete area, $A_c = \pi(a\text{-}t)(b\text{-}t)$, A_{cor} is the equivalent area effected by rebar stiffeners.

5.2 Formulation development

As shown in Fig. 14, the relationship between radial concrete stress ($\sigma_{r,c}$) in confined area and the transverse stress of the steel tube ($\sigma_{\theta,s}$) for both E-CFT and RE-CFT stub columns can be expressed a

$$\sigma_{r,c11} = \frac{t}{a-t}\sigma_{\theta,s} \tag{7}$$

$$\sigma_{r,c12} = \frac{t}{b-t}\sigma_{\theta,s} \tag{8}$$

So the relationship between mean radial concrete stress ($\sigma_{r,c}$) in confined area and the transverse stress of the steel tube ($\sigma_{\theta,s}$) is

$$\sigma_{r,c1} = \frac{(a+b-2t)t}{(a-t)(b-t)}\sigma_{\theta,s} \tag{9}$$

For RE-CFT stub columns, it is assumed that the confinement effect of elliptical steel tube and rebar-stiffeners on core concrete is independent. So the relationship of radial concrete stress generated by rebar-stiffeners ($\sigma_{r,c2}$) and yield strength of rebar-stiffeners (f_t) at the ultimate stage can be given as

$$\sigma_{r,c2} = \frac{f_t A_{ss0}}{A_{cor}} \tag{10}$$

where A_{ss0} is equivalent cross-section area of rebar-stiffeners, $A_{ss0} = \pi^2 d^2 l/(4S)$. And l is the total length of rebar-stiffeners all over the specimen. S is the spacing of stirrups along the height of the specimen.

For E-CFT stub columns, considering the lateral confinement stresses, the axial compressive stress of core concrete in the two regions can be expressed as

$$\begin{cases} \sigma_{L,c1} = f_c \\ \sigma_{L,c2} = f_c + k\sigma_{r,c1} \end{cases} \tag{11a}$$

And for RE-CFT stub columns, the axial compressive stress of core concrete in the three regions is

$$\begin{cases} \sigma_{L,c1} = f_c \\ \sigma_{L,c3} = f_c + p(\sigma_{r,c1} + \sigma_{r,c2}) \\ \sigma_{L,c4} = f_c + p\sigma_{r,c2} \end{cases} \quad (11b)$$

where p is the lateral pressure coefficient according to Ding *et al.* (2011b), p=3.4.

Based on the condition of the static equilibrium, the axial ultimate bearing capacity N_u for E-CFT stub columns can be given as

$$N_u = \sigma_{L,c1}A_{c1} + \sigma_{L,c2}A_{c2} + \sigma_{L,s}A_s \quad (12a)$$

For E-CFT stub columns, the axial ultimate bearing capacity N_u is

$$N_u = \sigma_{L,c1}A_{c1} + \sigma_{L,c3}A_3 + \sigma_{L,c4}A_{c4} + \sigma_{L,s}A_s \quad (12b)$$

Substituting Eqs. (4), (5), (6(a))-(11(a)) into Eq. (12(a)), N_u for E-CFT stub columns can be obtained as

$$N_u = f_cA_c + 1.1f_sA_s \quad (13a)$$

Substituting the data in Table 4 and Eqs. (6(b))-(11(b)) into Eq. (12(b)), N_u for RE-CFT stub columns can be obtained as

$$N_u = f_cA_c + 2.5f_tA_{ss0} + k'f_sA_s \quad (13b)$$

where k' is restraint coefficient of specimens.

The relationship between k' and ρ_v/ρ is listed in Table 4. According to the values of k' in Table 4, the restraint coefficient (k') of the specimens can be obtained by

$$k' = 1.1 + 2.4\frac{\rho_v}{\rho} - 14(\frac{\rho_v}{\rho})^2 \quad (14)$$

Meanwhile, fitted curve of restraint coefficient under various steel ratios and rebar stiffener ratios is shown in Fig. 16.

A comparison between Eqs. (13(a)) and (13(b)) suggests that the improvement of the ultimate bearing capacity of RE-CFT stub columns by rebar-stiffeners is attributable to the improvement of the ultimate bearing capacity of the concrete confined by rebar-stiffeners.

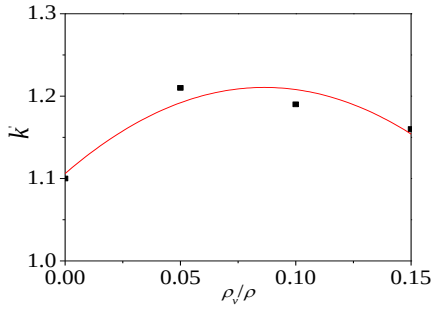

Fig. 16 Fitted curve of restraint coefficient (k') under various steel ratios and rebar stiffener ratios

5.3 Comparisons

Table 5 compares the load-bearing capacity obtained by FE modeling (i.e., $N_{u,1}$), Eq. (13) (i.e., $N_{u,2}$), and the experimental results (i.e. $N_{u,0}$) for all E-CFT and RE-CFT specimens. For E-CFT specimens, the average ratio of $N_{u,0}$ to $N_{u,1}$ obtained by FE modeling is 0.990 with a dispersion coefficient of 0.029, and the average ratio of $N_{u,0}$ to $N_{u,2}$ calculated by Eq. (13(a)) is 1.052 with a dispersion coefficient of 0.058. For RE-CFT specimens, the average ratio of $N_{u,0}$ to $N_{u,1}$ is 1.011 with a dispersion coefficient of 0.024, and the average ratio of $N_{u,0}$ to $N_{u,2}$ calculated by Eq. (13(b)) is 1.021 with a dispersion coefficient of 0.016. Therefore, both the proposed formula and the FE modeling results are in good agreement with the experimental results.

Fig. 17 presents the ultimate load-bearing capacities of both E-CFT and RE-CFT specimens obtained through the FE parametric studies in comparison with those obtained with the proposed formula. Satisfactory agreement was observed with the maximum discrepancy between E-CFT specimens and RE-CFT specimens at less than 10%.

For comparison purpose, Table 6 summarizes the current available guidance to calculate the ultimate bearing capacity of E-CFT stub columns. These formulas include the design guidance such as EC4 (2004) and CSA-S16-01 (2009) for normal CFT (rectangular and circle) columns which has been recommended for design of E-CFT stub columns. A unified axial compressive strength formula for E-CFT columns proposed by Zha *et al.* (2013) is also included.

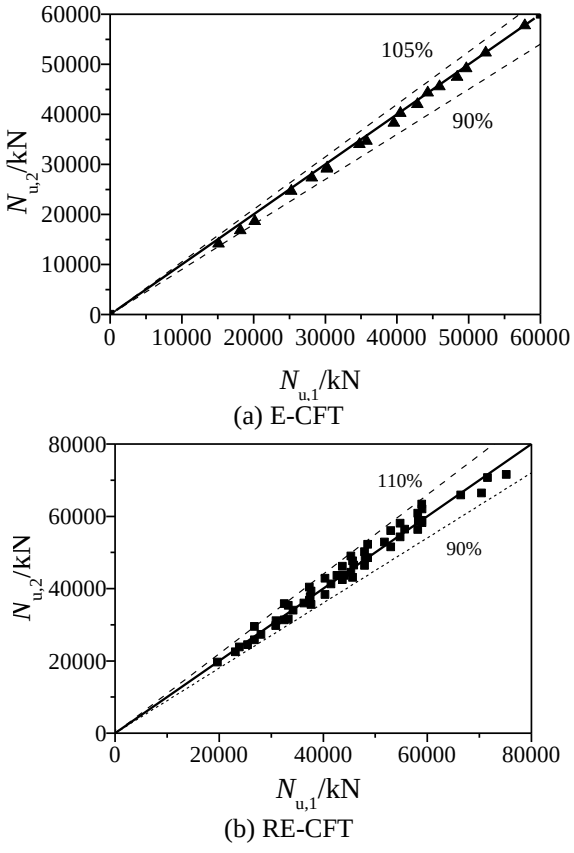

Fig. 17 Calculated results comparisons between $N_{u,1}$ and $N_{u,2}$

Table 5 Comparisons of the ultimate load-bearing capacity of E-CFT and RE-CFT stub columns obtained from experiments, FEA, and Eq. (13)

No.	Specimen label	$N_{u,0}$(kN)	$N_{u,1}$(kN)	$N_{u,2}$(kN)	$N_{u,0}$/ $N_{u,1}$	$N_{u,0}$/ $N_{u,2}$
1	OVST1-A	3100	2996	2739	1.035	1.132
2	OVST1-B	2860	2964	2711	0.965	1.055
3	OVST2-A	3690	3713	3432	0.994	1.075
4	OVST2-B	3810	3759	3474	1.014	1.097
5	OVST3-A	3900	3914	3631	0.996	1.074
6	OVST3-B	3900	3947	3716	0.988	1.050
7	OVST4-A	4390	4496	4377	0.976	1.003
8	OVST4-B	4110	4410	4424	0.932	0.929
		Average value			0.990	1.052
		Dispersion coefficient			0.029	0.058
9	OVRST5-A	3720	3676	3548	1.012	1.048
10	OVRST5-B	3610	3440	3567	1.049	1.012
11	OVRST6-A	4550	4563	4490	0.997	1.013
12	OVRST6-B	4500	4563	4453	0.986	1.011
		Average value			1.011	1.021
		Dispersion coefficient			0.024	0.016

Table 6 Summary of available formulas for ultimate bearing capacity of E-CFT stub columns

References	Formulas		Remarks
EC4(2004)	$N_u=\eta_a A_s f_y+A_c f_c'[1+\eta_c(t/D)(f_y/f_c')]$; $\eta_a=0.25(3+2\lambda)\le 1.0$; $\eta_c=4.9-18.5\lambda+17\lambda^2$; $N_{pl,RK}=A_s f_y+0.85A_c f_c'$; $(EI)_{eff}=E_s I_s+E_c I_c$; $\lambda=\sqrt{N_{pl,RK}/N_{cr}}$; $N_{cr}=\pi^2(EI)_{eff}/(k_e L)^2$	(15)	Circle
EC4(2004)	$N_u=A_s f_y+A_c f_c'$	(16)	Rectangle
CSA-S16-09(2009)	$N_u=\tau A_s f_y+\tau' \alpha_1 A_c f_c'$; $\rho=0.02(25-L/D)$; $\alpha_1=0.85-0.001 f_c\ge 0.67$; $\tau=1/\sqrt{1+\rho+\rho^2}$; $\tau'=1+(25\rho^2\tau/(D/t))(f_y/(\alpha_1 f_c'))$	(17)	Circle
CSA-S16-09(2009)	$N_u=A_s f_y+\alpha_1 A_c f_c$; $\alpha_1=0.85-0.001 f_c'\ge 0.67$	(18)	Rectangle
Zha *et al.* (2013)	$N_u=A_{sc} f_{sc}^k$; $A_{sc}=A_s+A_c$; $f_{sc}^k=(1+1.5(b/a)0.3\zeta)f_{ck}/(1+A_s/A_c)$	(19)	Elliptical

Eq. (13(a)) and the other available formulas in Table 6 were evaluated based on the ultimate bearing capacity of 8 E-CFT stub columns conducted in this paper and 32 such columns (a/b = 2) obtained from the literatures worldwide. These experimental data have covered a large range of geometric parameters and mechanical properties, such as $2a/t$ = 20.5 - 110.6, f_{cu} = 32.9 - 110.2 MPa, f_s = 311.0 - 424.4 MPa. The ultimate bearing capacity predicted by Eq. (13(a)) and other formulas in Table 6 are compared with the experimental results as shown in Table 7. It can be concluded that the results calculated by Eq. (19) are not safe compared with the experimental results. And Eq. (13(a)) developed in this study can conservatively predicted the results with higher accuracy in comparison with other available formulas.

Table 7 Comparison of the ultimate load-bearing capacity between experimental and predicted results

Specimen quantity and reference		Characteristic value	$N_{u,0}/N_{u,1}$	$N_{u,0}/N_{u,2}$					
				Eq.(13(a))	Eq.(15)	Eq. (16)	Eq. (17)	Eq. (18)	Eq. (19)
8	Yang *et al.* (2008)	Average value	0.970	0.953	0.956	0.978	1.045	1.090	0.892
		Dispersion coefficient	0.059	0.049	0.053	0.053	0.051	0.053	0.044
15	Zhao and Packer (2009)	Average value	1.011	1.009	1.005	1.045	1.095	1.153	0.940
		Dispersion coefficient	0.038	0.049	0.057	0.065	0.035	0.036	0.037
6	Jamaluddin *et al.* (2013)	Average value	1.007	1.017	1.074	1.122	1.173	1.242	0.955
		Dispersion coefficient	0.083	0.089	0.139	0.147	0.148	0.157	0.083
3	Zha *et al.* (2013)	Average value	1.016	1.075	1.050	1.102	1.118	1.188	1.003
		Dispersion coefficient	0.035	0.036	0.035	0.036	0.041	0.042	0.035
8	this paper	Average value	0.990	1.052	1.220	1.265	1.346	1.407	1.031
		Dispersion coefficient	0.029	0.058	0.069	0.069	0.083	0.079	0.058
40	total	Average value	1.006	1.017	1.052	1.092	1.149	1.207	0.956
		Dispersion coefficient	0.056	0.072	0.119	0.126	0.130	0.135	0.070

6. Conclusions

This paper investigated the compressive behavior of E-CFT and RE-CFT stub columns through experiments and numerical studies. The effects of the rebar-stiffeners on the mechanical performance of the RE-CFT columns were also studied. With the aids of the experimental results, a comprehensive parametric study was conducted and a simplified analytical approach was proposed to predict the ultimate bearing capacities of both E-CFT and RE-CFT stub columns. Based on the studies, the following conclusions can be drawn.

- The predicted results using FEA agreed well with the experimental results for both E-CFT and RE-CFT stub columns under compression. The numerical model can be used to accurately model both E-CFT and RE-CFT stub columns under axial loadings.
- It was found that the ultimate load-bearing capacity of RE-CFT stub columns was 20% higher than that of the E-CFT stub columns. Such improvement was attributed to the reinforcement effects from the internal rebar-stiffeners, which effectively enhanced the confinement effect on the core concrete, thereby significantly improved both the ultimate bearing capacity and the ductility of the E-CFT columns.

Based on the simplified stress nephogram, equations were developed to predict the ultimate bearing capacities of both E-CFT and RE-CFT stub columns under compression. The predicted results agreed well with both experimental and numerical results, and had much higher accuracy than other available methods.

Acknowledgments

This research work was financially supported by the National Natural Science Foundation of China, Grant No. 51578548.

References

CSA-S16-09, Canadian Standard (2009), Steel structures for buildings (limit states design), CAN/CSA-S16-09, Canadian Standards Association, Toronto, Ontario, Canada.

Dai, X.H., Lam, D. and Jamaluddin, N. (2014), "Numerical analysis of slender elliptical concrete filled columns under axial compression", *Steel Constr.*, 77(4), 26-35.

Dai, X. and Lam, D. (2010), "Numerical modeling of the axial compressive behavior of short concrete-filled elliptical steel columns", *J. Const. Struct. Res.*, **66**(7), 931-942.

Ding, F.X., Fang, C.J. and Bai, Y. (2014), "Mechanical performance of stirrup-confined concrete-filled steel tubular stub columns under axial loading", *J. Constr. Steel Res.*, **98**(7), 146-157.

Ding, F.X., Ying, X.Y. and Zhou, L.C. (2011a), "Unified calculation method and its application in determining the uniaxial mechanical properties of concrete", *Front. Archit. Civ. Eng.*, China, **5**(3), 381-393.

Ding, F.X., Yu, Z.W. and Bai, Y. (2011b), "Elasto-plastic analysis of circular concrete-filled steel tube stub columns", *J. Constr. Steel Res.*, **67**(10), 1567-1577.

EN 10210, European Standard (2006a), Hot finished structural hollow sections of non-alloy and fine grain steels—Part 1: Technical delivery conditions, EN 10210-1:2006(E), European Committee for Standardization, Brussels, Belgium.

EN 10210, European Standard (2006b), Hot finished structural hollow sections of non-alloy and fine grain steels—Part 2: Tolerances, dimensions and sectional properties, EN 10210-

2:2006(E), European Committee for Standardization, Brussels, Belgium.
Eurocode 4, European Standard (2004), Design of composite steel and concrete structures—Part 1-1: General rules and rules for buildings, EN1994-1-1, European Committee for Standardization, Brussels, Belgium.
GB/T228-2010, China Standard (2010), Metallic materials-tensile testing at ambient temperatures, Standards Press of China, Beijing, China.
GB/T50081-2016, China Standard (2016), Standard for method of mechanical properties on ordinary concrete, China Building Industry Press, Beijing, China.
GB50017-2014, China Standard (2014), Code for design of steel structures, China Planning Press, Beijing, China.
Hibbitt, Karlson & Sorenson Inc. (2014), ABAQUS/standard User's Manual, Version 6.4.1., Pawtucket, RI, USA.
Hua, W., Wang, H.J. and Hasegawa, A. (2014), "Experimental study on reinforced concrete filled circular steel tubular columns", *Steel Compos. Struct.*, **17**(4), 517-533.
Jamaluddin, N., Lam, D. and Dai, X.H. (2013), "An experimental study on elliptical concrete filled columns under axial compression", *J. Constr. Steel Res.*, **87**(8), 6-16.
Jiang, Z.G., Zhao, X. and Ren, Q.X. (2013), "Primary Analysis of Concrete-Filled Steel Tubular Slender Columns with Elliptical Section under Axial Compression", *Adv. Mater. Res.*, **671-674**, 736-739.
Li, H., Teng, J. and Li, Z. (2016), "Experimental study of damage evolution in cuboid stirrup-confined concrete", *Mater. Struct.*, **49**(7), 2857-2870.
Park, J.W. and Choi, S.M. (2013), "Structural behavior of CFRP strengthened concrete-filled steel tubes columns under axial compression loads", *Steel Compos. Struct.*, **14**(5), 453-472.
Qiu, W., Mccann, F. and Espinos, A. (2017), "Numerical analysis and design of slender concrete-filled elliptical hollow section columns and beam-columns", *Eng. Struct.*, **131**, 90-100.
Su, L., Wang, Y. and Cai, J. (2016), "Restoring Force Model of Concrete-Filled Square Steel Tubular Columns with Binding Bars", *Open Civ. Eng. J.*, **10**(1), 179-188.
Uenaka, K. (2014), "Experimental study on concrete filled elliptical/oval steel tubular stub columns under compression", *Thin. Wall. Struct.*, **78**(70) , 131-137.
Wang, Z.B., Tao, Z. and Han, L.H. (2017), "Strength, stiffness and ductility of concrete-filled steel columns under axial compression", *Eng. Struct.*, **135**, 209-221.
Xiamuxi, A., Hasegawa, A. and Suzuki, T.(2011), "Compression test of RCFT columns with thin-walled steel tube and high strength concrete", *Steel Compos. Struct.*, **11**(5), 72_43-72_51.
Yang, H., Lam, D. and Gardner, L. (2008), "Testing and analysis of concrete-filled elliptical hollow sections", *Eng. Struct.*, **30**(37), 71-81.
Yang, Y, Wang, Y. and Fu, F. (2014), "Effect of reinforcement stiffeners on square concrete-filled steel tubular columns subjected to axial compressive load", *Thin. Wall. Struct.*, **82**(9), 132-144.
Zha, X., Gong, G. and Liu, X. (2013), "Study on behavior of concrete filled elliptical steel tube members part I: short and long columns under axial compression", *Adv. Steel Constr.*, **9**(2), 90-107.
Zhao, X.L. and Packer, J.A. (2009), "Tests and design of concrete-filled elliptical hollow section stub columns", *Thin. Wall. Struct.*, **47**(6-7), 617-28.